ACS OMEGA

http://pubs.acs.org/journal/acsodf

Article

Novel Synthesis of CuO/GO Nanocomposites and Their Photocatalytic Potential in the Degradation of Hazardous Industrial Effluents

Farhana Anjum, Mohamed Shaban, Muhammad Ismail,* Saima Gul, Esraa M. Bakhsh, Murad Ali Khan,* Uzma Sharafat, Sher Bahadar Khan, and M. I. Khan

Cite This: *ACS Omega* 2023, 8, 17667−17681

Read Online

ACCESS | Metrics & More | Article Recommendations | Supporting Information

ABSTRACT: Photocatalytic degradation of dyes has been the subject of extensive study due to its low cost, eco-friendly operation, and absence of secondary pollutants. Copper oxide/graphene oxide (CuO/GO) nanocomposites are emerging as a new class of fascinating materials due to their low cost, nontoxicity, and distinctive properties such as a narrow band gap and good sunlight absorbency. In this study, copper oxide (CuO), graphene oxide (GO), and CuO/GO were synthesized successfully. X-ray diffractometer (XRD) and Fourier transform infrared (FTIR) spectroscopy confirm the oxidation and production of GO from the graphene of lead pencil. According to the morphological analysis of nanocomposites, CuO nanoparticles of sizes ≤20 nm on the GO sheets were evenly adorned and distributed. Nanocomposites of different CuO:GO ratios (1:1 up to 5:1) were applied for the photocatalytic degradation of methyl red (MR). CuO:GO(1:1) nanocomposites achieved 84% MR dye removal, while CuO:GO(5:1) nanocomposites achieved the highest value (95.48%). The thermodynamic parameters of the reaction for CuO:GO(5:1) were evaluated using the Van't Hoff equation and the activation energy was found to be 44.186 kJ/mol. The reusability test of the nanocomposites showed high stability even after seven cycles. CuO/GO catalysts can be used in the photodegradation of organic pollutants in wastewater at room temperature due to their excellent properties, simple synthesis process, and low cost.

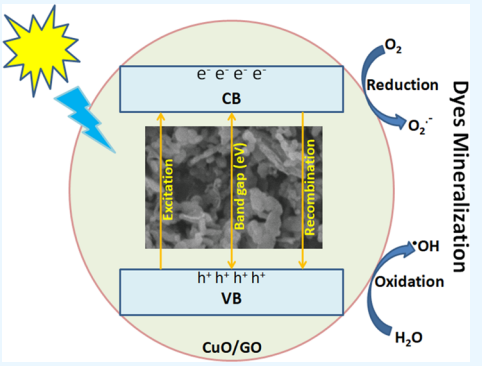

INTRODUCTION

Biodegradability of organic dyes and their potential carcinogenic effects on human health have made them well-known as hazards to the environment. These dyes unquestionably possess great technological properties.[1] However, their interaction might result in dermatitis, discomfort, severe respiratory tract irritation, rupture of the nasal septum, skin ulcers, and severe diarrhea.[2] Furthermore, organic dyes hurt marine life and have serious negative effects on water quality. It is estimated that between 10 and 15% of the colors used in the textile industry are lost during production each year. Industrial waste effluents are extremely poorly biodegradable, with a highly variable chemical composition, a strong color, and a changing pH level. Because of this, cationic dyes are extremely challenging to eliminate using current procedures. Purification of wastewater containing dyes poses a severe danger to public health and aquatic ecological sustainability.[3] To attain acceptable drinking water quality, effective technology for eliminating color and toxicity from textile effluents is required. The significance of wastewater treatment and management has raised substantial issues for scientific research and public health in recent years. A more efficient way to get rid of these toxins combines all of the existing procedures (physical, chemical, and biological).[4] Due to its ease, low cost, and lack of toxicity, adsorption is one of the most promising physical methods for eliminating these dyes.[5,6] However, toxins cannot be completely extracted or degraded when this procedure is performed alone; instead, they are concentrated via absorption and become impossible to remove from the environment. Other methods that are frequently used to remediate contaminated wastewater include chemical oxidation, membrane filtration, coagulation/flocculation, and mixing processes.[7] On the other hand, photocatalytic oxidation is one of the most effective ways to remove dyes and other impurities from water because it can completely mineralize these substances and convert them to less volatile H_2O and CO_2 without causing secondary contamination and requires little energy for maintenance.[8] The use of a heterogeneous

Received: January 8, 2023
Accepted: April 6, 2023
Published: May 5, 2023

photocatalyst for purifying water is a common method that involves oxygen molecules, hydroxyl anions, or other organic molecules for oxidation and reduction reactions.[9] As photocatalysts, several semiconductors such as TiO_2, ZnO, and others have been employed because they are nontoxic, chemically stable, widely accessible, and cost-effective.[10,11] Practical uses of these photocatalysts have been limited by intrinsic properties such as poor quantum yield and high band gap, restricting their utility in visible-light applications. Since particle recovery is a complicated process or a daunting operation, this approach is very costly. To boost the solar efficiency of photocatalysts under visible-light irradiation, the nanomaterials must be modified to facilitate visible-light absorption. Synthesizing photocatalysts with new materials as catalytic support without compromising their efficiency is a viable alternative. Many studies have shown that when nanoparticles are infused or layered with larger particles such as semiconductors, noble metals, and polymeric materials, the rate of charge recombination is reduced. Now, we need to design and develop single-phase oxide photocatalyst materials that could be worked under visible-light illumination.[12] Photocatalysts are now being immobilized on adsorbents such as carbon, zeolite, clays, and other materials by different researchers and these integrated photocatalysts are being used to degrade the toxic organic dyes in the presence of solar light.[13] This combination not only keeps all of the fascinating qualities of each element but it also overcomes important drawbacks, including weak absorptivity and photogenerated electron recombination.[14] That is why polymer-based nanocomposites have received greater attention in both the academic world and industries.[15] Graphene is a two-dimensional transparent material made up of sp^2-C atoms arranged in a hexagonal lattice. Graphene and its functionalized nanocomposites have lately received a lot of attention due to their large and active surface area as well as their excellent carrier mobility. Because of the presence of adequate oxygen-containing functional groups, oxidized graphene, also known as graphene oxide, shows to be more reactive, making the synthesis of GO derivative compounds simpler.[16] The formation of GO, which offers a fast and convenient reduction route, results in the development of a new sp^2 hybrid by removing an oxygen atom.[17] According to Dong et al., graphene-based metal-oxide nanocomposites have gained widespread attention due to their remarkable electrocatalytic activity, electrochemical energy conversion, and electrochemical sensing characteristics.[18] This makes GO nanocomposites a promising material for a wide range of applications, including gas detectors,[19] lithium-ion batteries,[20] and catalytic applications.[21] It is envisaged that the nanocomposite formation of graphene with the metal-oxide nanoparticles improves the intrinsic characteristics of graphene by increasing the charge transfers between metal oxides and organic dye molecules.[22] Sarkar and Dolui synthesized copper oxide/reduced GO nanocomposites and demonstrate that they exhibited excellent and sustained catalytic activity,[23] while Choi et al. assessed the photocatalytic activity of semiconductor CuO/rGO nanocomposites under visible-light irradiations in the degradation of methylene blue dye.[24] CuO is a native p-type semiconductor material with an indirect theoretical band gap of 1 eV and an experimental narrow band gap of ∼1.2 eV. CuO possesses special chemical and physical properties, like excellent solar light absorbance, and a large specific surface area, making the material useful in several fields.[25] Inspired by these properties, we were interested to produce high-quality CuO nanoparticles decorated on the GO surface to fabricate nanocomposites through the sonochemical route. It is reported that graphene-based nanocomposites can absorb light in the visible region and which makes it very useful in many environmental applications including the design of excellent catalysts for the removal of different industrial effluents from wastewater.[26] These properties were the inspiration for the synthesis of CuO/GO nanocomposites and their usage as a catalyst in environmental applications.

As a continuation of recent efforts in the green synthesis of metal-oxide nanoparticles,[6,11,27] in the present work, we have synthesized graphene oxide and CuO/GO nanocomposites. As graphene/metal-oxide nanohybrids can bring visible light into environmental applications, they also function well as a photocatalyst for the removal of organic dyes such as methyl orange (MO), methylene blue (MB), methyl red (MR), eosin (EO), and Alizarin red (AR). As a consequence, it provides a solid foundation for making CuO/GO and returning it to nature through use as a photocatalyst for environmental uses.

2. EXPERIMENTAL SECTION

2.1. Materials Used. The chemicals used were cupric chloride ($CuCl_2.2H_2O$), acetic acid (CH_3COOH), sodium borohydride ($NaBH_4$), sodium hydroxide (NaOH), methyl red ($C_{15}H_{15}N_3O_2$), methylene blue ($C_{16}H_{18}ClN_3S$), eosin dye ($C_{20}H_6Br_4Na_2O_5$), alizarin ($C_{14}H_8O_4$), sulfuric acid (H_2SO_4), hydrochloric acid (HCl), potassium permanganate ($KMnO_4$), hydrogen peroxide (H_2O_2), phosphoric acid (H_3PO_4), and potassium hydroxide (KOH). All of these chemicals were purchased from Sigma-Aldrich and were used without any additional purification. Pencil lead was obtained from the local market. For washing purposes, analytical-grade methanol, ethanol, and acetone were used. The reaction tubes were wrapped in aluminum foil.

2.2. Synthesis of Graphene Oxide. GO was synthesized using a modified version of the well-known Hummer technique. In detail, 2 g of pencil lead powder was mixed with 46 mL (98% purity) of concentrated sulfuric acid and 1 g of $NaNO_3$ before being sonicated for 1 h in an ultrasonicator. Following that, 6 g of $KMnO_4$ was added to the reaction combination over a period of 2 h. After that, the mixture was heated at 35° C for 18 h, the reaction mixture was chilled in an ice bath, and 40 mL of water was also added. A blackish-brown coloration was observed. At this time, the reaction was quenched by introducing hydrogen peroxide. The solution was then rinsed with 0.5% hydrochloric acid to eliminate the sulfate ion.[22,28] The final product of GO was then dried at 75 °C and stored for future use.

2.3. Preparation of CuO Nanoparticles. The wet precipitation method was used to synthesize CuO nanoparticles from $CuCl_2{\cdot}2H_2O$ solution (0.2 M) and NaOH (0.2 M aqueous solution) in deionized water. For CuO synthesis, 100 mL of copper chloride solution was mixed with 1 mL of glacial acetic acid and heated to 100 °C while continuously stirring. After that, sodium hydroxide solution was gradually added dropwise to the heated solution, stirring constantly until the color change was observed from green to black. The formation of black color confirmed CuO nanoparticles in the solution mixture. After centrifugation, the precipitate was washed with distilled water and then dried in an open atmosphere for 24 h.[29] The nanoparticles were calcined for 4 h at 500 °C.

https://doi.org/10.1021/acsomega.3c00129
ACS Omega 2023, 8, 17667−17681

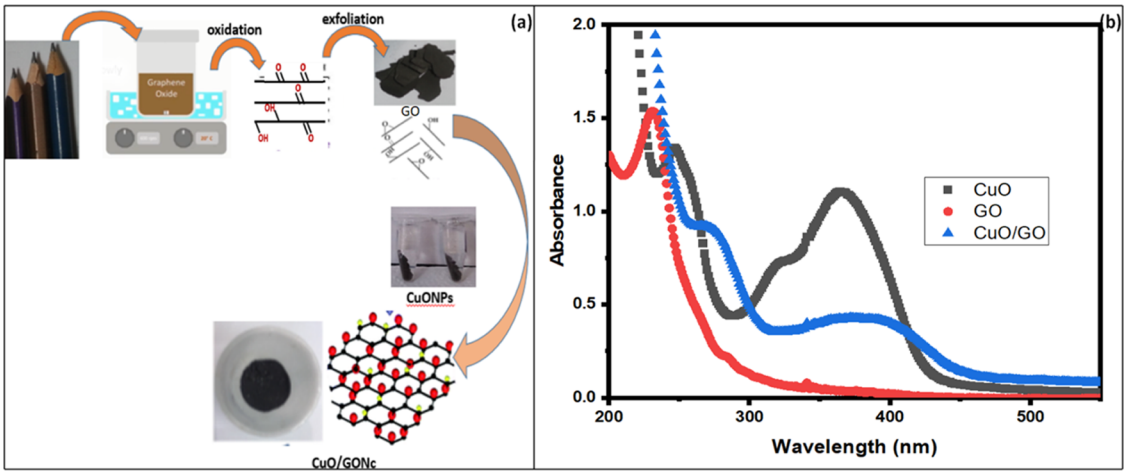

Figure 1. (a) Mechanism of CuO/GO nanocomposites synthesis ("Photograph courtesy of "Farhana Anjum"; Copyright 2022"). (b) UV−vis absorption spectra of GO, CuO, and CuO/GO nanocomposites.

The chemical reaction is

$$CuCl_2 + 2NaOH \rightarrow Cu(OH)_2 + 2NaCl \quad (1)$$

$$Cu(OH)_2 \rightarrow CuO + H_2O \quad (2)$$

2.4. Preparation of CuO/GO Nanocomposites. For the synthesis of CuO/GO (1:1) nanocomposites, 2 g of CuO was suspended in 40 mL of distilled water and then 2 g of GO was added. This mixture was ultrasonicated (50 Hz) for 1 h at an ambient temperature in an ultrasonic system. The mixture was heated to 80 °C for 2 h and then chilled to room temperature. CuO/GO nanocomposites were collected by centrifugation/filtration and dried at 100 °C.

2.5. Photocatalytic Activity Experiments. Degradation studies of various organic dyes were conducted by using a visible-light catalytic process. The light source used was a 200 W HID xenon light bulb H1 (HCDLT China) positioned 15 cm from the catalyst surface. A UV−visible Shimadzu-UV-1800 analyzer was used to assess the photodegradation efficacy of CuO/GO, CuO, and GO. MR was used as a model dye to evaluate the efficiencies of all of these materials and nanocomposites with various composite ratios.

In this experiment, 50 mg of the catalyst (1 mg/mL) was added to 50 mL of dye solution (25 μg/mL) and stirred in the dark for 1 h at room temperature to make sure the adsorption equilibrium between the catalyst and the dye. In this way, the adsorption and desorption stabilities of the dye on the surface of the photocatalyst were achieved before illumination. After reaching equilibrium, the first aliquot (2−3 mL, 0 min) was examined for its UV/vis absorbance. At regular time intervals during the irradiation, aliquots of 2−5 mL were taken and examined for their UV/visible absorbance after centrifugation. Changes in absorption were used to track the decolorization of MR dye using a UV−visible spectroscopy analytical approach.[30]

To check the stability of our catalysts, the nanocomposite was centrifuged, cleaned, dried, and reused in recycling experimentation for the photodegradation studies of dyes at the same concentration.

2.6. Characterization. Different characterization methods were used to identify the various characteristics of the produced catalysts. The functional groups, morphologies, elemental compositions, and crystallinities of the prepared catalysts were determined by using a FT-IR, Spectrum-100FT-IR, Broker, ALPHA and a field emission scanning electron microscope (FE-SEM, JSM-7600F, JEOL, Japan) equipped with an energy dispersive X-ray (EDX) unit and an X-ray diffractometer (XRD). The UV−visible Shimadzu-UV-1800 Spectrometer was used to determine the optical characteristics of the samples.

3. RESULTS AND DISCUSSION

3.1. CuO/GO Nanocomposites Synthesis. The CuO/GO nanocomposites was synthesized by ultrasonication of CuO with GO sheets at room temperature and pressure using an ultrasonic bath (Figure 1a). For nanocomposites, the two solutions of CuO and GO were mixed and sonicated at 80 °C for 30 min. CuO/GO formation was confirmed by the appearance of a blackish-brown precipitate. The agglomeration tendency of graphene in water due to $\pi-\pi$ stacking interactions can be prevented by the addition of functional groups or metal oxide. Graphene functionalization improves the characteristics by altering the GO's surface structure, allowing for increased dispersion in solvents. The metal-oxide nanocomposite built on graphene has excellent electrochemical detection and electrocatalytic characteristics.[17,18] All of these properties combine to make it the most effective catalyst for the complete mineralization of industrial dyes.[31] On the other hand, CuO nanoparticles have been identified as one of the most promising metal oxides for the growth on the surface of graphene oxide because CuO and its nanoparticles are known to have exceptionally high thermal conductivities.[32] These qualities motivated us to develop high-quality CuO nanoparticles on the GO surface to manufacture nanocomposites via the sonochemical route, i.e., these properties were the inspiration for the synthesis of CuO/GO nanocomposites by precipitation and Hammer approaches and their usage as catalysts for environmental applications.

3.2. Physicochemical Characterization Studies of CuO/GO. The UV-visible spectrum of GO depicted two absorption peaks; one at ∼238 nm and the other is a shoulder at ∼285 nm, which corresponds to C═O bonds (n−π transitions) (Figure 1b). The main absorption peak at ∼238 nm is π to π^* transitions of aromatic (C═C) double bonds of GO. The UV absorption spectrum of CuO/GO nanocomposites also has two unique absorption peaks at 279 and

https://doi.org/10.1021/acsomega.3c00129
ACS Omega 2023, 8, 17667−17681

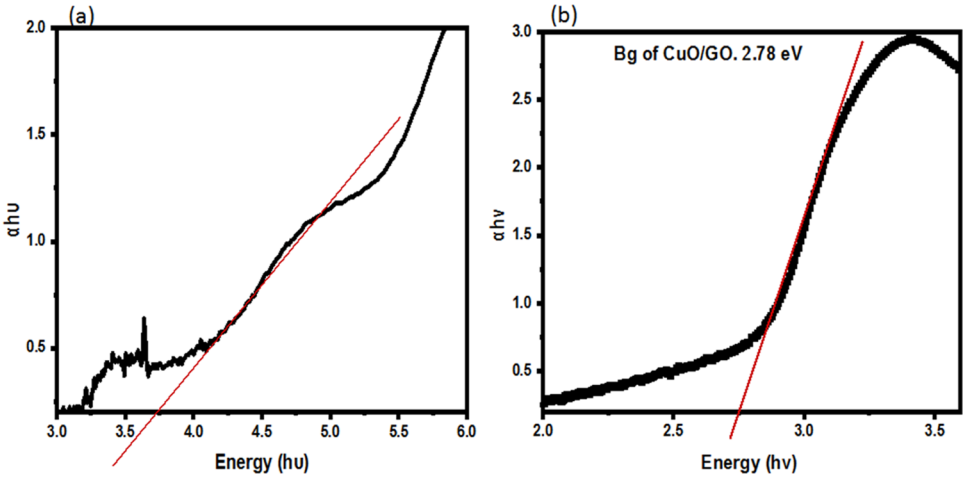

Figure 2. (a) Tauc plot of CuO NPs and (b) Tauc plot of CuO/GONc.

389 nm, which are related to π plasmon excitation of the graphitic structure and CuO, respectively. The graphitic peak at ∼238 nm red-shifted to ∼279 nm because of the extension of conjugation. For CuO nanoparticles, two absorption bands, a broad band at 243 nm and the other band at around 369 nm, were obtained, ascribing the interband transition of central electrons of Cu metal and CuO nanocrystals. These results are in parallel with earlier studies.[33] Its anisotropic character was shown by two or more bands that were formed as a result of quadrupole and multiple plasmon excitations. The characteristic absorption peak of CuO NPs is affected by the GO in CuO/GO nanocomposites. It is clear from Figure 1b that the spectrum of the composite is red-shifted when compared to pure CuO. However, by increasing the concentration of CuO up to a certain level, visible-light absorbance is gradually reduced. This increase in visible-light absorption of CuO/GO nanocomposites could be due to the greater surface electric charge of oxides. The CuO nanoparticles typically exhibit a maximum optical absorption peak of ∼350 nm. The main absorbance peak of CuO nanoparticles has moved to a shorter wavelength (300 nm), indicating structural alterations in CuO nanoparticles.[33]

3.3. Band Gap Energy of CuO/GO Nanocomposites. Tauc's relation was used to calculate the optical band gap energy of CuO nanoparticles

$$\alpha h\upsilon = (h\upsilon E_g)^n \quad (3)$$

where "'$h\upsilon$'" is the incident photon energy, and "'n'" specifies the type of transition that causes absorption; its values depend on whether the transition is direct or indirect. Its value is 1/2 or 2. Using the Tauc relation, CuO NPs were able to attain an optical band gap energy (E_g, eV) of 3.7 eV (Figure 2a), which was greater than the corresponding value for bulk CuO (2.1 eV).[34] The decreased particle size is responsible for the increased Eg value, making CuO NPs an ideal solar energy harvester and a powerful photocatalyst for pollutant removal.[35] The band gap energy of CuO nanoparticles was estimated to be 3.7 eV, while this band gap is reduced to 2.78 eV band gap energy by uploading CuO nanoparticles on the GO surface to form CuO/GO nanocomposites (Figure 2b). This shows that Eg decreases as the particle size increases due to aggregation and formation of composites. When photons hit a semiconductor material, they are only absorbed if their minimum energy is sufficient to excite an electron to the conducting band from the valence band, which is equivalent to the band gap energy (E_g). The increase in surface charge between CuO and GO causes the optical band gap to shift to a greater wavelength, resulting in a reduction, in the band gap of CuO/GO.[33]

3.4. FT-IR Spectra of GO, CuO, and CuO/GO Nanocomposites. FT-IR is the basic tool for the identification of functional groups. O−H stretching vibrations are responsible for the large and broadened peak centered at 2900−3599 cm^{-1} in the GO FT-IR spectrum; see Figure S1.[36] While the peaks around 1590 and 1055 cm^{-1} are attributed to the sp^2-hybridized C═C and C−O stretching, respectively,[37] while, peaks at 1067 and 1400 cm^{-1} were assigned to the stretching vibration of unreacted graphite C−O and C═C bonds. The symmetric and asymmetric stretching is confirmed by the presence of these epoxy groups.

The FT-IR spectrum of the CuO/GO nanocomposites also showed the presence of CuO NPs along with GO. After the synthesis of CuO/GO nanocomposites, peak intensities at 2900−3599, 1067, and 1400 cm^{-1} are reduced, revealing that during nanocomposites formation, the majority of oxygen-containing functional groups, notably carboxyl groups, were reduced. Moreover, the typical FT-IR spectrum of CuO presents peaks at 3400, 2930, 1550, 1040, and 610 cm^{-1}. The Cu−O stretching vibration causes the absorption peak at 610 cm^{-1} in the FT-IR of pure GO and CuO/GO nanocomposites.

3.5. XRD of GO, CuO, and CuO/GO Nanocomposites. In the XRD, GO exhibited a strong diffraction peak at $2\theta \sim 10.4°$ (Figure 3). This dominant diffraction peak at about 10.4° corresponds to the (002) diffraction plane of GO, having a basal spacing of d [002] = 8.2626 Å.[38] A very small diffraction peak of reduced GO at around 26.7° (calculated spacing ≈ 3.3 Å) was also observed. The broader diffraction peak observed in the enlarged pattern of GO and the significant increase in the spacing attributed to the oxygen functional group intercalates in the graphite interlayer. The interlayer distance was enhanced by the introduction of various functional groups, including C−O, C−OOH, and C−OH, resulting in a higher value of GO basal spacing. Figure 3 also illustrates the XRD pattern of the prepared CuO nanoparticles, which reveals a single monoclinic phase. Diffraction peaks at 32.28, 35.24, 38.44, 48.46, 53.26, 58.1, 61.32, 65.96, and 67.84° are assigned to the (011), (111), (111), (202), (020), (202), (113), (311), and (220) respectively, diffraction planes

https://doi.org/10.1021/acsomega.3c00129
ACS Omega 2023, 8, 17667−17681

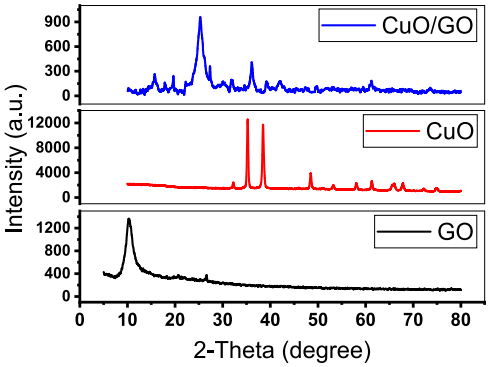

Figure 3. XRD patterns of GO, CuO, and CuO/GO nanocomposites.

of monoclinic CuO.[39] The structure's lattice parameters are a = 4.84 Å, b = 3.47 Å, and c = 5.33 Å, which agree well with the standard JCPDS card no. 00-044-0706.[40] Previously, similar results were reported by Guzman et al.[41] and Ganga et al.[42] These XRD patterns do not show any impurity peak. Because of the nanosize effect, peaks are broad and wide. The average crystallite size of the prepared CuO NPs is 25.85 nm, calculated by using the well-known Scherer equation.

The broad diffraction peak at 10.3° in the CuO/GO XRD pattern is apparently due to the (002) planes of the hexagonal GO structure as seen in Figure 3. The peaks at 12.18, 25.6, 38.3, 44.5, and 50.2° correspond to the (011), (111), (200), (112), and (202) diffraction planes of monoclinic CuO in the CuO/GO composite. The average crystallite size of CuO in the composite is ~26.41 nm.

3.6. SEM Microscopy of GO, CuO, and CuO/GO Nanocomposites. The nanoparticle sizes and nanomorphologies of GO, CuO, and CuO/GO nanocomposites were observed by TEM and SEM images. Figure 4a,b illustrates the perfect exfoliation of graphite to generate thin layers of GO. The TEM images of GO are orientated like folded silk veil waves nanosheets that ripple and entangle with each other. The van der Waal interactions account for the lamella-like structure of wrinkled graphene oxide nanosheets. The lateral dimensions of these sheets, which are typically transparent, range from hundreds of nanometers to several micrometers. In these wrinkles, GO sheets can be observed, which range in size from 5 to 10 μm, indicating 100% oxidation. Figure 4c,d

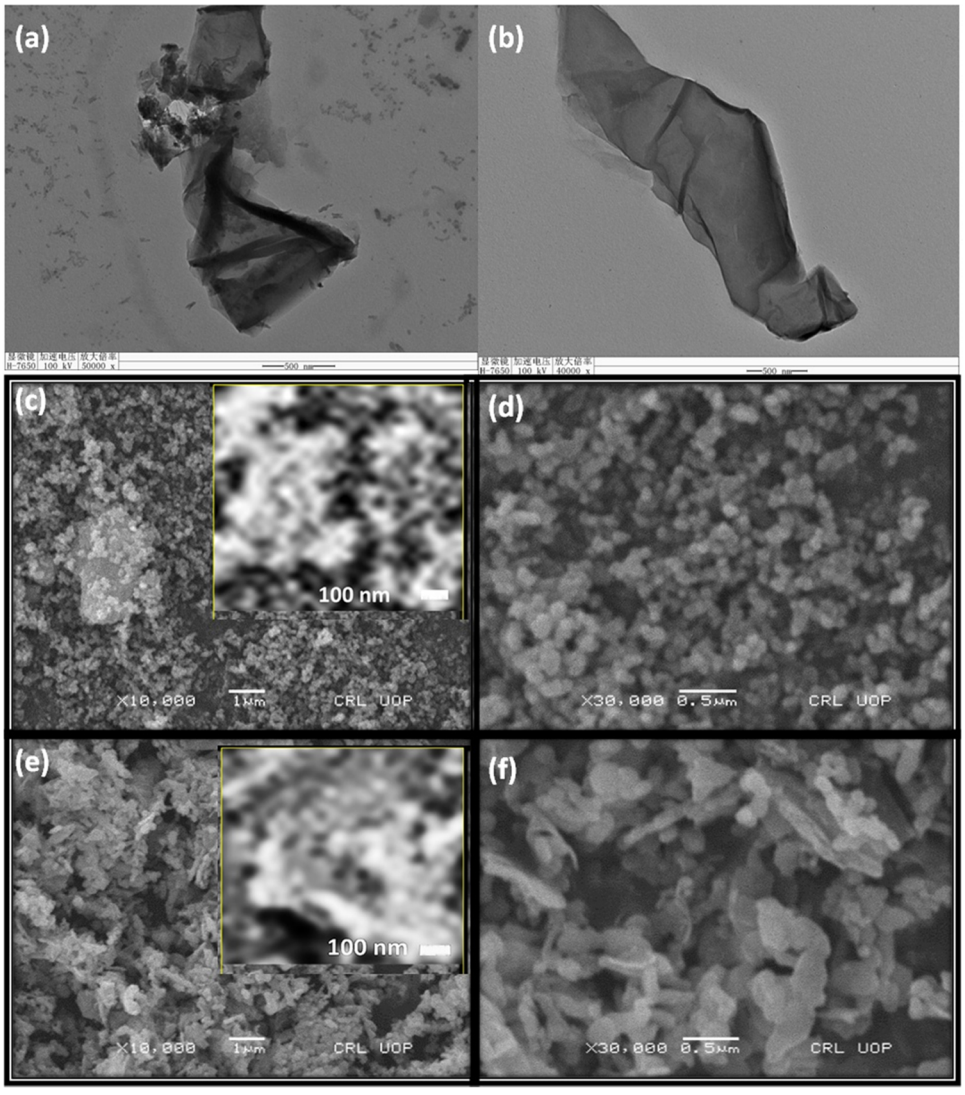

Figure 4. (a, b) TEM images of GO,[22] (c, d) SEM images of CuO NPs, and (e, f) SEM images of CuO/GO nanocomposites.

https://doi.org/10.1021/acsomega.3c00129
ACS Omega 2023, 8, 17667−17681

depicted the morphology of extremely crystalline CuO nanoparticles from SEM analysis. An aggregation of nanoparticles with an average diameter between 18 and 20 nm was visible in the SEM image. Thus, only a rough morphology was identified from this observation.

The copper oxide nanoparticles are evenly distributed over GO's crumpled, paper-like surface, as seen in SEM illustrations of CuO/GO, indicating that CuO nanoparticles are incorporated into GO (Figure 4e,f). CuO particles in CuO/GO nanocomposites are varied from 32 to 90 nm with an average value of about 39.66 nm and are uniformly distributed on the graphene layer, preventing it from agglomeration. There are two types of morphologies: spherical form CuO and wrinkled sheet-like form of GO, indicating that CuO NPs are firmly attached to the surface of these sheets. The particle size of CuO NPs measured by SEM images was identical to the crystallite size determined by XRD.

3.7. EDX Analysis. The purity and elemental makeup of nanomaterials were assessed using EDX analysis and presented in Figure S2. The purity of synthesized CuO NPs was confirmed by the EDX spectrum in Figure S2a. It indicates that copper is either oxide or dioxide and that the nanoparticles were nearly stoichiometric. The weight composition for copper and oxygen was 82.97 and 15.70%, respectively. The atomic composition of copper and oxygen was then calculated as 56.17 and 42.21%, respectively. CuO has a uniform distribution of copper and oxygen with an atomic ratio of 1:1.[43] The EDX of GO (Figure S2) shows the C and O signals at 0.5 and 0.8 keV, with a ratio of 1.315 to 2.161, indicating the purity of GO.[44]

The EDX analysis confirmed the formation of CuO and GO nanocomposites with a 5:1 ratio, Figure S2. According to the EDX spectra, the weight percentage of copper, oxygen, and carbon in the CuO/GO composite were 60.56, 14.08, and 5.59% by weight while being 36.01, 33.25, and 17.57% atomic percentages, respectively. CuO/GO hybrid nanocomposites formation was verified by EDX spectra at similar weight percentages of 7.85 and 6.89% for CuO and GO, respectively. Extra peaks like Zn, Si, and Mn can also be observed, which may be due to the glassware used. The strong intensities and condensed breadth of these peaks suggested that the resulting materials were mostly crystalline in nature.[45] Single small peak for Cl in the CuO sample, Pt in GO, and Mn and Zn signals in the composite may be due to the impurity of the lead pencil or arise in the simple glass slides or detected error during measurements.

3.8. Applications. *3.8.1. Photocatalytic Properties.* At present, dyes are produced and used widely throughout many different industries, including printing, garments, paper, pulp, etc. However, the amount of dyestuffs discharged into aqueous habitats, endangers both human health and aquatic life.[27,46] In recent decades, nanomaterials have been successfully employed to photocatalyst the mineralization of commercial dyes such as methylene blue and naphthol blue black.[1,47] The nanocatalyst was applied for the degradation studies of different dyes (Table 1).

3.8.2. Selectivity of the Dye. The catalytic effectiveness of the prepared CuO/GO nanocomposites was evaluated against five different dyes, including MO, MB, MR, EO, and AR. The efficacy of CuO/GO nanocomposites against different dyes is shown in Figure 5a. The catalytic efficiency of CuO/GO nanocomposites reached 97.80, 88.57, 92.97, and 91.46% for MO, AR, MB, and ES dyes degradation, respectively, in 120 min. However, the studied composite revealed a degradation efficiency of 84.01% for MR in 175 min, even though MR is a necessary dye from an industrial perspective and is used in a variety of industries, including coloring textiles, clay products, leather printing ink, pharmaceutical industries, and as a filter in photography. Furthermore, due to its high carcinogenicity and resistance to photodegradation and complete mineralization, it required a very long time to decay. Therefore, to increase the photodegradation effectiveness of our proposed nanocomposites and decrease the reaction time to efficiently degrade the MR dye, numerous reaction-related parameters, such as concentration, pH, and temperature, must be tweaked in the following sections.

Table 1. Catalytic Mineralization of Methyl Red by Different Reported Catalysts

s. no.	catalyst	rate of reaction	refs
1	ZnO	0.0534	48
2	Ag^{+}-doped TiO_2	0.1103	49
3	TiO_2	0.0492	49
4	Au^{+}-doped SiO_2NPs	0.370	50
5	Ag^{+}-doped SiO_2 NPs	0.50	50
6	AgNPs-deposited SiO_2 NPs	0.046	50
7	AuNPs−AgNPs-deposited SiO_2NPs	0.037	50
8	AuNPs-deposited SiO_2NPs	0.032	50
9	SiO_2 NPs	0.020	50
10	Fe^0/UV	1.06	51
11	Fe^{2+}/UV	0.05	51
12	Fe^0/APS/UV	1.59	51
13	Fe^{2+}/APS/UV	0.56	51
14	Fe^0/H_2O/UV	8.56	51
16	Fe^{2+}/H_2O/UV	1.21	51
17	Ag 2.0/TiO_2	0.0069	52
18	ZnS/CdS nanocomposites	1.818	53

3.8.3. Comparative MR Degradation by GO, CuO, and CuO/GO Nanocomposites. Comparative photocatalytic degradation of MR was assessed by using GO, CuO, and CuO/GO nanocomposites upon exposure to UV/sunlight irradiation. The photocatalytic efficiency of all of these catalysts against MR is shown in Figure 5b. Because MR dye is resistant to self-photolysis, a slight drop in MR dye concentration was observed as a result of dye adsorption on the catalyst surface. In 175 min, GO and CuO demonstrate respective efficiencies of 62.55 and 67.23%. These findings demonstrate that CuO/GO nanocomposites, with an efficiency of 84.01% in 175 min, outperforms other nanomaterials in the degradation of the MR dye. The progressive decline in intensity without the emergence of a new absorption peak proved that the chemical intermediates generated during dye degradation did not absorb any analytical wavelengths. CuO/GO nanocomposites demonstrated sufficient activity to photocatalyst mineralization of MR dye due to their tiny particle size and large surface area. Allowing more contact with the mutagenic disruption of the chemical structure of the MR dye improves the photocatalytic properties of GO and increases its photocatalytic activities. CuO/GO is the best catalyst, according to the analysis of CuO, GO, and CuO/GO nanocomposites in the photodegradation of the MR dye.

3.8.4. MR Degradation by Different CuO/GO Composite Ratios. CuO/GO nanocomposites have been synthesized with five different CuO to GO ratios (1:1 up to 5:1) via the direct solution precipitation method, the same as CuO/GO was

https://doi.org/10.1021/acsomega.3c00129
ACS Omega 2023, 8, 17667−17681

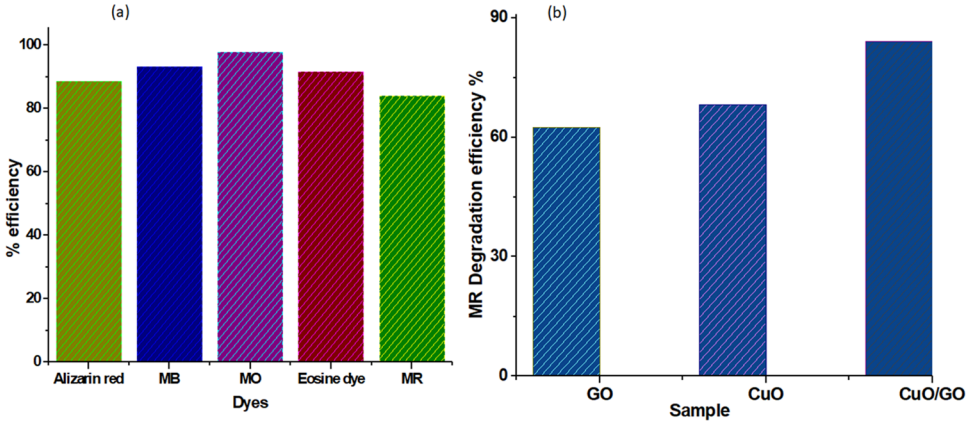

Figure 5. (a) Photocatalytic degradation of alizarin red, methylene blue, methyl orange, eosin dye, and methyl red by CuO/GO nanocomposites and (b) degradation efficiency of MR dye by GO, CuO, and CuO/GO nanocomposites.

prepared. The prepared samples were represented as 1:1, 2:1, 3:1, 4:1, and 5:1 CuO/GO, respectively. As in the previous example, the photocatalytic decomposition efficiencies of these prepared nanomaterials were determined using the same MR dye solution and examined by a UV double-beam spectrophotometer (Shimadzu-UV-1800). Before irradiation, the reaction was vigorously stirred in complete darkness for at least 1 h to attain the adsorption equilibrium between the MR dye and CuO/GO nanocomposites. After light irradiation, at a given time interval, 5 ml aliquots were collected for analysis and subsequently the absorbance spectra were recorded. The sample was analyzed in the 200−800 nm UV range wavelength. Time-dependent UV−visible absorbance spectra of the aforementioned reaction in the presence of CuO/GO nanocatalyst at different ratios of CuO to GO are shown in Figure 6. These observations suggest that the optical properties of CuO NPs may be tuned by the presence of GO.

Photodegradation of the MR dye follows first-order kinetics as already reported in the literature.[22] These results are consistent with those seen in the photodegradation of the majority of organic compounds, especially azo dyes. As predicted, increasing the number of active sites in CuO/GO favorably influenced photocatalytic degradation kinetics. Behind 5:1, an increase in metal-oxide concentrations does not accelerate the decolorization efficiency of MR because of two reasons: (i) agglomeration might have taken place and (ii) higher concentration creates turbidity parallel to the Langmuir adsorption isotherm. Using the Langmuir−Hinshelwood kinetics model, the photocatalytic decolorization rate of MR was evaluated, as seen below

$$\ln C_0/C_t = k_{app}\cdot t \quad (4)$$

where C_0 is the initial MR concentration, C_t is the final concentration in mg/L, and t is the irradiation time in minutes. Photocatalytic degradation of methyl red follows the first-order rate, its apparent rate (k_{app} in min^{-1}) has been determined using the graph's slope when $\ln(C_0/C_t)$ was plotted against time (t), as presented in Figure S3a. The calculated series of k_{app} was 0.0068 min^{-1} for CuO/GO (1:1), 0.0094 min^{-1} for CuO/GO (2:1), 0.0174 min^{-1} for CuO/GO (3:1), 0.0202 min^{-1} for CuO/GO (4:1), and 0.0258 min^{-1} for CuO/GO (5:1). With increased CuO concentration of 5:1, k_{app} increases to its maximum value. These results show that at the start, the reaction proceeds slowly by catalyst only, but when the reaction mixture was exposed to sunlight, the reaction rate increased tremendously by holding more photons and thus produces more $OH^{\bullet}$ radicals, which are abundant and easily accessible to the nearby MR molecules for decolorization/degradation. Thus, k_{app} is increasing due to the increase in the overall surface area of the CuO/GO nanocatalyst.

The results of photocatalytic mineralization of MR at various nanocomposites ratios agree well with the Langmuir−Hinshelwood model. It also suggests that this process follows the first-order kinetic law. Values of linear regression (R^2) for MR mineralization of various nanocomposites ratios vary from 0.906 to 0.957, as presented in Figure S3a. The 5:1 composite ratio has the greatest k_{app} value of 0.0258 min^{-1}. Similar concentration-dependent photodegradation tendencies of the MB dye have previously been described by Jeyabalan et al.[54] and Vanaja et al.[55]

Experimental data in Table 2 shows that the photodegradation rate of the MR has increased from 84.01 to 95.48%. Furthermore, increasing the composite ratio from 1:1 to 5:1 reduces the reaction time from 3.5 h to only 35 min. Another intriguing feature is that the removal rate reduced as the ratio was increased beyond 5:1. According to the Langmuir−Hinshelwood model, (a) agglomeration occurs at increasing concentrations, which may lower the number of active surface sites available for absorption and (b) turbidity is caused by increased concentration. Turbidity is a scattering effect that reduces light penetration. As a result, an appropriate composite ratio might have decreased particle size and improved crystallinity. The removal rate has therefore improved.

3.8.5. Initial Dye Concentration of MR vs CuO/GO Nanocomposites. The effect of initial dye concentration on the photocatalytic decomposition rate is depicted in Figure 7a. The rate of reaction was studied by varying the concentration of MR, while keeping all other experimental conditions constant such as light intensity, CuO/GO nanocatalyst dosage (0.5 mg) and composite ratio (5:1), and MR solution pH (6.5 almost neutral). While using varying initial MR concentrations of 90, 100, and 120 ppm, all of these reactions were conducted at room temperature. These results show that the rate of the photocatalytic reaction decreases and vice versa when the starting MR concentration increases because the CuO/GO photocatalyst's surface is covered in numerous layers of dye molecules that have been adsorbed. As a result, increasing the MR dye content has no beneficial effect on further decolorization. The MR molecules can no longer engage

https://doi.org/10.1021/acsomega.3c00129
ACS Omega 2023, 8, 17667−17681

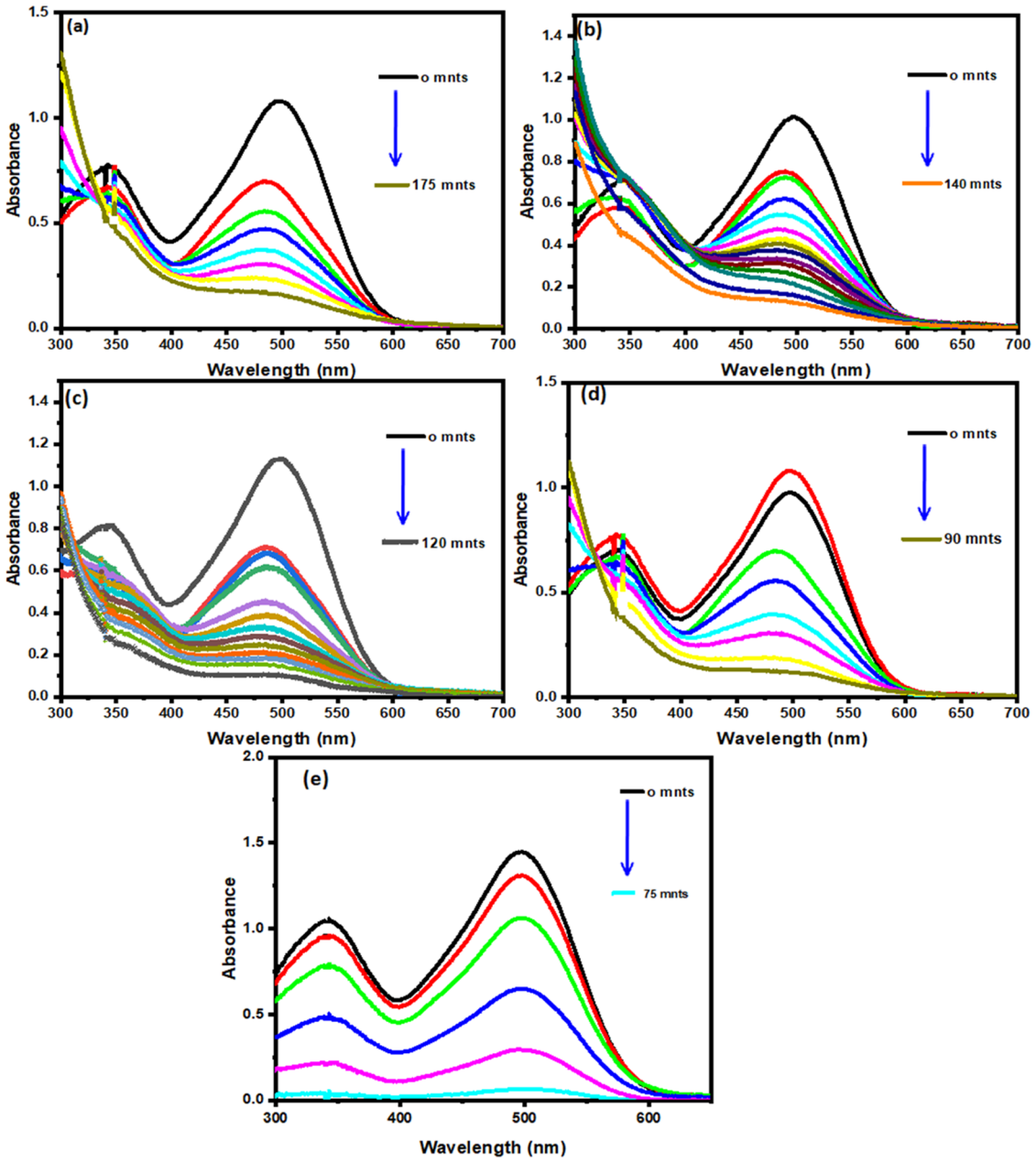

Figure 6. Photocatalytic mineralization of the MR dye by different composition ratios of CuO/GO nanocomposites: (a) 1:1, (b) 2:1, (c) 3:1, (d) 4:1, and (e) 5:1.

Table 2. Rate of Reaction, Efficiencies, Turnover Numbers, and Turnover Frequencies of CuO/GO Nanocomposites of Different Composition Ratios: 1:1, 2:1, 3:1, 4:1, and 5:1

composite ratio (CuO/GO)	k_{app} (min^{-1})	efficiency (%)	turnover number (TON)	turnover frequency (TOF)	linear regression coefficients (R^2)
1:1	0.0068	84.01	16.1	0.092	0.9579
2:1	0.0094	86.98	21.95	0.156	0.9324
3:1	0.0174	88.41	23.5	0.195	0.9459
4:1	0.0202	90.77	23.6	0.262	0.9333
5:1	0.0258	95.48	25.5	0.340	0.9066

with the CuO/GO nanocatalyst surface due to these adsorbed layers. The photodegradation reaction is thus inhibited because the fresh incoming MR dye molecules have very limited access to hydroxyl ($OH^{\bullet}$) and oxygen ($O_2^{\bullet}$) free radicals, which are generated at the surface of the CuO/GO nanocatalyst. According to Beer–Lambert's law, increasing the MR dye concentration also shortens the photon's access path to the MR solution, resulting in a lower penetration of radiations to the CuO/GO nanocatalyst and consequently lowering the rate of reaction. This behavior could be for two possible reasons: (i) when the MR dye solution concentration increases, (ii) the path length of the photon increases, so that the photon number reaching the surface also decreases, and hence a limited number of superoxide ions (O_2^-) and hydroxyl ($OH^{\bullet}$) radicals were formed, thus decreasing the rate of reaction. As the surface area of the CuO/GO photocatalyst is fixed, the photocatalytic degradation rate is dependent on the dye concentration. Since there are a limited number of active sites in this system that induce a lower number of adsorption of MR

https://doi.org/10.1021/acsomega.3c00129
ACS Omega 2023, 8, 17667−17681

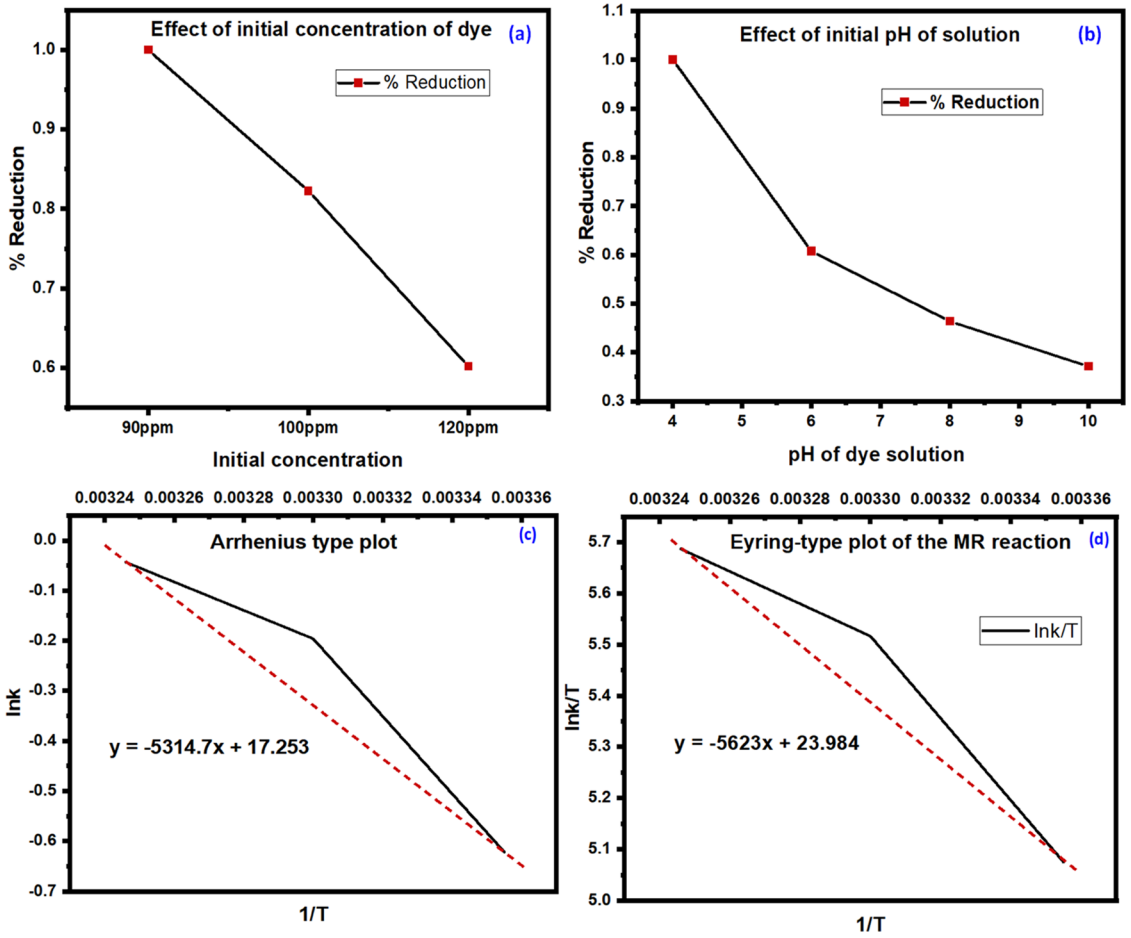

Figure 7. (a) Effect of MR dye concentration and (b) pH on the degradation of MR in the presence of the CuO/GO catalyst. (c) Arrhenius plot by plotting $\ln(k)$ as a function of $1/T$ and (d) Eyring plot of $\ln(k/T)$ vs $1/T$.

molecules at these active catalyst surfaces, the remaining MR molecules stay in solution until the previously attached MR molecules have degraded. But in the case of a higher concentration, the competition rate is also high among the MR dye molecules. More MR molecules will try and compete with each other for the attachment to the CuO/GO catalyst active site, and this results in reducing the MR degradation rate. Due to a lack of direct contact between MR molecules and the active site, it is thought that the presence of such a large amount of adsorbed MR molecules may negatively affect the reaction rate and the production of photogenerated holes or $OH^{\bullet}$.[56]

3.8.6. Effect of pH on MR Degradation. The pH of the dye effluents is a significant parameter for the CuO/GO surface charge properties, MR adsorption activity, and, subsequently, the rate of photodegradation reaction. As a result, it is critical to look at the effect of pH on photocatalytic degradation and figure out what pH is optimum for the degradation of MR treatment. The influence of pH on photocatalytic reactions might be explained using zero-point charge (pzc) of the CuO/GO photocatalyst and also the adsorption of MR molecules on CuO/GO nanocatalyst at various pH values. The CuO/GO photocatalyst isoelectric point relies on the acid−base properties of the hydroxyl surface group. The isoelectric point is the pH at which the zeta potential is zero. Under acidic conditions, it is believed that adsorbed H^+ charges on the photocatalyst surface positively (pH < 5.6) while negatively charged with the presence of alkaline media (pH > 5.6), when the surface of the CuO/GO nanocatalyst absorbed OH^- ions as shown in the following reaction

$$(\mathrm{CuO/GO}) - \mathrm{OH} + \mathrm{OH}^- \leftrightarrow (\mathrm{CuO/GO}) - \mathrm{O}^- + \mathrm{H_2O} \quad \text{at pH} > \text{pzc} \tag{5}$$

The cationic and anionic composition greatly influences the efficiency of this reaction. Different electrostatic forces, attraction, or repulsion between MR molecules and the CuO/GO surface either boost or reduce this efficiency. Results plotted in Figure 7b suggest that the rate of photocatalytic degradation increases when the pH of the solution decreases but reduces when the pH is increased.

In acidic media, i.e., pH < 5.6, the surface of the CuO/GO photocatalyst is charged positively by the surface species ($\mathrm{CuO/GO{-}OH_2^+}$) and can strongly interact with negatively charged organic compounds

$$(\mathrm{CuO/GO}) - \mathrm{OH} + \mathrm{H}^+ \leftrightarrow (\mathrm{CuO/GO}) - \mathrm{OH_2}^+ \quad \text{at pH} < \text{pzc} \tag{6}$$

These results showed that MR photodegradation is affected by acidic or alkaline media rather than the zero-point charge (pH = pzc) of the CuO/GO photocatalyst. Since the electric charge density is zero at pH = 5.6 on the surface of the CuO/GO photocatalyst, the constant (K) was calculated from the first-order kinetic plot.[57]

https://doi.org/10.1021/acsomega.3c00129
ACS Omega 2023, 8, 17667−17681

Table 3. Estimated Values for E_a, Δ^*H, Δ^*S, and Δ^*G in kJ/mol

T (K)	$1/T$	K (s^{-1})	ln K	E_a (kJ/mol)	Δ^*H (kJ/mol)	Δ^*S (kJ/mol)	Δ^*G (kJ/mol)
298	0.00335	0.537	−0.6217	44.186	46.749	1.86	−507.541
303	0.00330	0.8212	−0.196				−563.831
308	0.00324	0.9577	−0.0432				−526.131

3.8.7. Thermodynamic Functions of the CuO/GO Nanocomposites in the Degradation of MR. The velocity of gas molecules increases as the temperature increases according to the KMT. This is also true for any liquid. A molecule's translational kinetic energy is directly related to the molecule's velocity (K.E = $1/2mv^2$). The K.E consequently increases along with the temperature. The percentage of molecules high enough to break the energy barrier increases along with the increase in temperature. The percentage of molecules whose energy exceeds the activation energy (E_a) overcomes the energy barrier and produces the final product.

The impact of different temperatures (293, 303, 308, and 313 K) on MR dye photodegradation by CuO/GO was investigated in this section. The k_{app} of these reactions at different temperatures was determined. It was found that as the temperature increased, the degradation efficiency increases as well. Arrhenius's equation relates k_{app} and temperature by following eq 7

$$k = Ae^{-E_a/RT} \tag{7}$$

where "k" is the rate constant, "E_a" is the activation energy, "R" is the universal gas constant, "T" is the temperature in Kelvin, and "A" is the Arrhenius factor/frequency factor or preexponential factor. The Arrhenius equation may be projected onto a straight line to graphically compute activation energy

$$\ln(k) = -E_a/RT + \ln A \tag{8}$$

Plotting $\ln(k)$ as a function of $1/T$ results in a straight line with a slope of $(-E_a/R)$ as presented in Figure 7c. E_a can be simply calculated from this slope. This increasing rate constant is most likely due to increased collision frequency among molecules in the solution medium as the temperature increases.

Other thermodynamic functions like enthalpy of activation (ΔH^*) and entropy of activation (ΔS^*) have been determined by Eyring's equation, activation energy (E_a) and apparent rate of reaction (k_{app}) are related to each other by the following equation

$$k_{app} = (K_B T/h)e^{-\Delta * S/R} \times e^{-\Delta * H/RT} \tag{9}$$

The linear form of the Eyring−Polanyi equation is obtained by differentiating the above equation concerning temperature as follows

$$\ln(k_{app}/T) = \ln K_B/h + \Delta * S/R - \Delta * H/RT \tag{10}$$

Below, Figure 7d shows an Eyring plot of the MR dye degradation process.

ΔH (46.749 kJ/mol) has been calculated from the slope while ΔS (1.86 kJ/mol) from the intercept of the above graph, respectively. Lastly, ΔG was determined using Arrhenius Law according to eq 11

$$\Delta * G = \Delta * H - T\Delta * S \tag{11}$$

The results of E_a, Δ^*H, Δ^*S, and Δ^*G values in kJ/mol are presented in Table 3.

The increase in the k_{app} value with increasing temperature and the positive value of ΔH demonstrate that the photodecomposition of MR by the CuO/GO nanocomposites is an endothermic process. This might be owing to the hydrophobic CuO/GO nanocatalyst's electrostatic attraction to the MR dye. At the higher temperature, the large negative Δ^*G value suggested that the reaction is favorable and spontaneous. Positive values of Δ^*S refer to the affinity of CuO/GO nanocomposites toward MR dye as presented in Table 4.

Table 4. Conditions for Spontaneity of the Reaction

ΔH	ΔS	ΔG	spontaneity of reaction
+ve	+ve	depending on T, may be +ve or −ve	yes if T is high
−ve	+ve	always −ve	always spontaneous
−ve	−ve	depending on T, may be +ve or −ve	yes, if T is low enough
+ve	−ve	always +ve	never spontaneous

3.9. Heterogeneous Catalysts. Two different tests, including the mercury poisoning test and a hot filtration test, were conducted to ascertain whether the CuO/GO nanocomposites degrades MR in a heterogeneous or homogeneous way.

3.9.1. Hot Filtration Test. Under typical conditions, the MR degradation process was carried out in the presence of the CuO/GO catalyst. After a while, when the pigment had only undergone 30% of its degradation, the solid catalyst was filtered out, and the reaction was left to proceed in the light for 2 days. No further deterioration of MR was observed even after 2 days in the light, indicating that the catalyst (CuO/GO) was heterogeneous in character.[58]

3.9.2. Mercury Poisoning Test. The heterogeneity of CuO/GO nanocatalysts as catalytically active species under typical reaction circumstances was evaluated using the mercury poisoning (drop) test. The degradation process of MR was stopped by CuO/GO when a small drop of mercury was introduced to it while it was being constantly stirred. Because mercury amalgamated on the surface of the heterogeneous photocatalyst, the reaction was halted due to a lack of an active site on the surface.[59]

Both tests yielded positive results, confirming that the catalysts are heterogeneous and this reaction is heterogeneous in nature.

3.10. Stability of the Photocatalyst. Apart from the other qualities of the CuO/GO nanocomposites, the catalyst's stability is one of the most essential properties in large-scale applications.[60] To determine if the CuO/GO(5:1) catalyst is stable, MR dye recycling experiments were carried out, and the results are presented in Figure S3b. Before being dried in an oven at 80 °C, the produced nanocomposites catalysts were centrifuged and washed with distilled water, and then ethanol after each cycle was completed and then employed in the subsequent reaction. After seven cycles, the MR dye removal rate for CuO/GO nanocomposites decreased from 90.90% to 84.9% as presented in Figure S3b. The graph shows a slight decline in CuO/GO photocatalytic activity. This is due to the

https://doi.org/10.1021/acsomega.3c00129
ACS Omega 2023, 8, 17667−17681

Scheme 1. Mechanisms of Photodegradation of MR Dye by CuO/GONc ("Scheme Courtesy of "Farhana Anjum"; Copyright 2022")

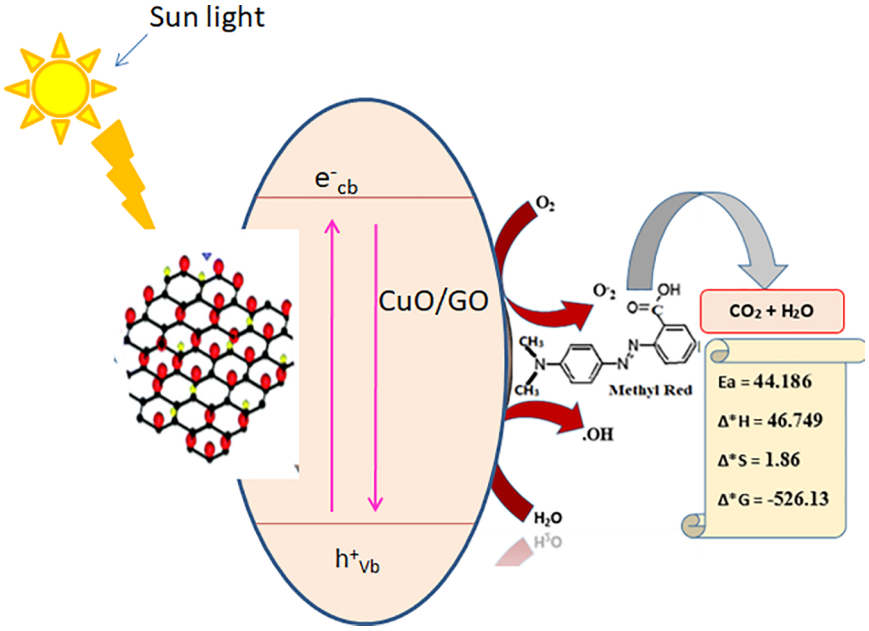

mechanical loss of the nanocatalyst surface that occurs during the cyclic process. As a result, nanocomposites' photocatalytic degradation activity and stability have remained high for a long period.

3.11. Degradation of Mixed Dyes Solutions by the CuO/GO Nanocomposites. In addition to the degradation of pure dyes solution, other reactions for a combination of dyes solutions were conducted against CR, MO, and MR solution. In this experiment, 60 mg of the catalyst was added to 60 mL of a mixture of dyes (20 mL of each dye), and the mixture was stirred at room temperature for 10 min in dark conditions. After 10 min, the first aliquot (3 mL, 0 min) was examined with a UV−visible spectrophotometer. Throughout light irradiation, an aliquot of 4 mL was centrifuged and examined with a UV−visible spectrometer at regular intervals of 20 min. As shown in Figure S4, the aqueous CR, MO, and MR solution produced an absorbance peak at 473 nm. The highest intensity at 473 nm gradually diminishes over time. The degradation of CR, MO, and MR dyes is indicated by the reduction in the peak intensity at 473 nm for CR, MO, and MR solution and the emergence of a new peak at 249 nm with increasing intensity. As a consequence, it took 190 min for the combination of CR, MO, and MR dyes to degrade by 94%. Based on the aforementioned findings, it was determined that our CuO/GO nanocomposites preparation is not only efficient in the degradation of a single dye solution but also exhibits admirable activity in the degradation of a mixture of dyes solution and may be used in the degradation/purification of the actual water-containing dyes solution.

3.12. Photolysis of the MR Dye by CuO/GO Nanocomposites. *3.12.1. Indirect Dye Degradation Mechanism.* A schematic representation of MR photocatalysis by the CuO/GO nanocomposites is illustrated in Scheme 1 and provides a plausible mechanism for MR degradation reaction 12. The proposed mechanism of the reaction is given: photocatalytic processes are usually triggered by irradiation of light as a result of photoelectrons increased from the valence band (VB) of the CuO/GO catalyst to the conducting band (CB). The energy of this light that has been absorbed is now equal to or greater than the photocatalyst band gap energy (E_g).The valence band developed a hole as a result of photoelectron excitation. Thus, as stated in the equation below, pair of electrons and holes (e^-/h^+) are generated

$$\mathrm{CuO/GO} + h\nu \rightarrow \mathrm{CuO/GO}(e^-(\mathrm{CB}) + h^+(\mathrm{VB})) \quad (12)$$

The formation of hydroxyl radicals, which occurs when water ionizes and reacts with the newly created hole in the valence band to produce a hydroxyl radical (OH^-), is another process by which MR molecules degrade

$$H_2O + h^+(\mathrm{VB}) \rightarrow OH^{\bullet}(\mathrm{ads}) + H^+(\mathrm{ads}) \quad (13)$$

This CuO/GO surface $OH^{\bullet}$ radical is a very potent oxidizing agent that attacks adsorbed MR molecules that are close to the catalyst surface and mineralized to the degree that depends on the structure and their stability nonselectively. These hydroxyl radicals can kill any existing microorganisms in the medium in addition to attacking organic pollutants.[61] Similarly, the excited electrons in the conducting band now interact with the nearby oxygen to create anionic superoxide radical (O_2^-), as in eq 14

$$O_2 + e^-(\mathrm{CB}) \rightarrow O_2^-(\mathrm{ads}) \quad (14)$$

These superoxide radicals aid in the oxidation process while also preventing the recombination of electrons and holes, keeping the CuO/GO catalyst's electron neutrality.

Superoxide is protonated in this step, which results in the production of H_2O_2. During the prior step, superoxide ions were formed. These further dissociate and produce a hydroxyl radical, which is very volatile. The oxidation and reduction reactions occur concurrently on the photoexcited CuO/GO catalyst surface in photocatalysis. Scheme 1 shows the complete procedure.

3.12.2. Direct Mechanism for Dye Degradation. Due to the ability of CuO/GO catalyst to absorb some of the visible light too, another mechanism of photodegradation of MR dye

https://doi.org/10.1021/acsomega.3c00129
ACS Omega 2023, 8, 17667−17681

is also possible under visible light. In this mechanism, the MR molecules absorb the visible-light photons (1 > 400 nm) and get excited from the ground state to the excited state (MR*), in this triplet excited state, the MR molecules further convert to a semioxidized radical cation (MR*) due to some electrons in the CB of CuO/GO.[62] Now, these trapped electrons react with dissolved oxygen and form superoxide radical anions (O_2^-), which results in the formation of hydroxyl radicals ($OH^•$). Now, these hydroxyl radicals ($OH^•$) are the prime factor in the degradation of MR dye molecules as represented by the below equation[63]

$$MR + h\nu \rightarrow MR^* \quad (15)$$

$$MR^* + CuO/GO \rightarrow MR^+ + CuO/GO^- \quad (16)$$

According to several reported studies, an indirect mechanism typically prevails over a direct mechanism, and its contribution to MR degradation is far more pronounced than the one initiated by visible light. The latter is also considered to be a much slower reaction than the indirect mechanism.[63]

3.12.3. Mineralization Study of MR. Analyses of the total organic carbon (TOC) are frequently used to determine how thoroughly organic dye molecules are broken down during photodegradation. TOC can more accurately represent the total amount of organic compounds in the solution by measuring the amount of carbon in organic compounds. A TOC analyzer was used to assess the TOC of the original dye solution (blank) and irradiated sample. Equation 17 was used to evaluate the competence of TOC removal[64]

$$R(\%) = 100 \times (TOC_{0e} - TOC_t)/TOC_{0e} \quad (17)$$

where TOC_{0e} is the TOC value at sorption equilibrium time and TOC_t is the TOC value after irradiated time t.

As shown in Figure S5, the degradation of MR was demonstrated using CuO:GO(5:1) and CuO:GO(1:1) photocatalysts. Under visible-light irradiation, the CuO:GO(5:1) photocatalyst exhibited better MR photodegradation competence than CuO:GO (1:1) photocatalyst. This is due to the increased ability of O2 to adsorb molecules, which allows for the creation of reactive radicals. The equilibrium content of the MR dye after 30 min of adsorption in the dark was found to be 23.25 mg·L^{-1}. After 180 min of irradiation with a 200 W xenon lamp, final TOC values in the presence of CuO:GO (1:1) and CuO:GO (5:1) were 3.45 and 8.34 mg·L^{-1}, respectively. The percent value of TOC of the CuO:GO(5:1) system decreased to 14.83%, showing high mineralization of the MR dye with a removal efficiency of 85.16%, while the percent TOC value of the CuO:GO(1:1) system was only 35.8% with the removal efficiency of 64.13%.

4. CONCLUSIONS

This paper describes the novel lead pencil-based synthesis of reduced graphene oxide and its composites with copper oxide. This study proposed a new type of photocatalyst that possessed superior photocatalytic activity in very short reaction times for the degradation of the industrial organic MR dye. CuO/GO was synthesized by the sonochemical method, while GO was synthesized by modifying the hammer method. The effectiveness of each method was evaluated based on textural, morphological, and structural characterizations of obtaining nanopowders and nanocomposites that are performed by different modern methods. The photocatalytic efficiency of the nanocomposites depends on the amount of GO associated with CuO. The CuO/GO nanocomposites with 5:1 was found to achieve the highest ∼90.90% removal efficiency of MR under visible-light irradiation in 70 min. These high values of photocatalytic efficiency of CuO/GO could be attributed to the improved charge passage and separation that suppressed charge recombination, longer charge lifespan (stability), and the enrichment of photon absorption. The proposed technique could be used for the production of several nanocomposites materials, with many others conducting polymers that can be used for the present-day environmental issue of pollution caused by numerous carcinogenic organic pollutants.

■ ASSOCIATED CONTENT

Supporting Information

The Supporting Information is available free of charge at https://pubs.acs.org/doi/10.1021/acsomega.3c00129.

FT-IR spectra of GO, CuO, and CuO/GO nanocomposites (Figure S1); EDX spectra of (a) CuO, (b) GO, and (c) CuO/GO nanocomposites (Figure S2); (a) fitting plots based on the first-order kinetics model for MR photodegradation using nanocomposites of different CuO/GO ratios: (a) 1:1, (b) 2:1, (c) 3:1, (d) 4:1, and (e) 5:1, and (b) stability of CuO/GO photocatalyst versus the number of reusability cycles (Figure S3); photocatalytic degradation of the CuO/GO nanocomposites against a mixture of CR, MO, and MR dyes [60 mL of aqueous dyes solution (20 mL each dye) + 60 mg of CuO/GO (5:1) nanocomposite] (Figure S4); and TOC removal % of MR using CuO:GO (5:1) and CuO:GO (1:1) under visible-light irradiation (Figure S5) (PDF)

■ AUTHOR INFORMATION

Corresponding Authors

Muhammad Ismail − *Department of Chemistry, Kohat University of Science & Technology, Kohat 26000 Khyber Pakhtunkhwa, Pakistan;* orcid.org/0000-0002-8185-0511; Email: ismailkust@yahoo.com

Murad Ali Khan − *Department of Chemistry, Kohat University of Science & Technology, Kohat 26000 Khyber Pakhtunkhwa, Pakistan;* orcid.org/0000-0002-8286-5504; Email: drmalikhan@yahoo.com

Authors

Farhana Anjum − *Department of Chemistry, Kohat University of Science & Technology, Kohat 26000 Khyber Pakhtunkhwa, Pakistan*

Mohamed Shaban − *Physics Department, Faculty of Science, Islamic University of Madinah, Al Madinah Al Monawara 42351, Saudi Arabia; Nanophotonics and Applications (NPA) Lab, Physics Department, Faculty of Science, Beni-Suef University, Beni Suef 62514, Egypt;* orcid.org/0000-0002-4368-8269

Saima Gul − *Department of Chemistry, Kohat University of Science & Technology, Kohat 26000 Khyber Pakhtunkhwa, Pakistan*

Esraa M. Bakhsh − *Chemistry Department, Faculty of Science, King Abdulaziz University, Jeddah 21589, Saudi Arabia*

Uzma Sharafat − *School of Science and the Environment, Grenfell Campus, Memorial University of Newfoundland and Labrador, Corner Brook, Newfoundland A2H 5G4, Canada*

https://doi.org/10.1021/acsomega.3c00129
ACS Omega 2023, 8, 17667−17681

Sher Bahadar Khan − *Chemistry Department, Faculty of Science, King Abdulaziz University, Jeddah 21589, Saudi Arabia;* orcid.org/0000-0001-9635-7175

M. I. Khan − *Department of Chemistry, Kohat University of Science & Technology, Kohat 26000 Khyber Pakhtunkhwa, Pakistan*

Complete contact information is available at: https://pubs.acs.org/10.1021/acsomega.3c00129

Notes

The authors declare no competing financial interest.

Institutional Review Board Statement: This study, conducted in this project, did not involve humans or animals.

■ ACKNOWLEDGMENTS

This research work was funded by the Institutional Fund Projects under Grant No. IFPIP: 221-247-1443. The authors gratefully acknowledge technical and financial support provided by the Ministry of Education and King Abdulaziz University, DSR, Jeddah, Saudi Arabia.

■ REFERENCES

(1) Hassanpour, M.; Salavati-Niasari, M.; Mousavi, S. A.; Safardoust-Hojaghan, H.; Hamadanian, M. CeO2/ZnO ceramic nanocomposites, synthesized via microwave method and used for decolorization of dye. *J. Nanostruct.* **2018**, *8*, 97−106.

(2) Ismail, M.; Akhtar, K.; Khan, M.; Kamal, T.; Khan, M. A.; M Asiri, A.; Seo, J.; Khan, S. B. Pollution, Toxicity and Carcinogenicity of Organic Dyes and their Catalytic Bio-Remediation. *Curr. Pharm. Des.* **2019**, *25*, 3645−3663.

(3) (a) Hou, J.; Li, X.; Yan, Y.; Wang, L. Electrochemical Oxidation of Methyl Orange in an Active Carbon Packed Electrode Reactor (ACPER): Degradation Performance and Kinetic Simulation. *Int. J. Environ. Res. Public Health* **2022**, *19*, 4775. (b) Ismail, M.; Khan, M. I.; Khan, S. B.; Akhtar, K.; Khan, M. A.; Asiri, A. M. Catalytic reduction of picric acid, nitrophenols and organic azo dyes via green synthesized plant supported Ag nanoparticles. *J. Mol. Liq.* **2018**, *268*, 87−101. (c) Sabri, M.; Habibi-Yangjeh, A.; Rahim Pouran, S.; Wang, C. Titania-activated persulfate for environmental remediation: the-state-of-the-art. *Catal. Rev.* **2021**, 1−56.

(4) (a) Zhang, J.; Zhang, H.; Chen, L.; Fan, X.; Yang, Y. Optimization of PNP Degradation by UV-Activated Granular Activated Carbon Supported Nano-Zero-Valent-Iron-Cobalt Activated Persulfate by Response Surface Method. *Int. J. Environ. Res. Public Health* **2022**, *19*, 8169. (b) Akhundi, A.; Habibi-Yangjeh, A.; Abitorabi, M.; Rahim Pouran, S. Review on photocatalytic conversion of carbon dioxide to value-added compounds and renewable fuels by graphitic carbon nitride-based photocatalysts. *Catal. Rev.* **2019**, *61*, 595−628.

(5) Khan, M.; Ali, S. W.; Shahadat, M.; Sagadevan, S. Applications of polyaniline-impregnated silica gel-based nanocomposites in wastewater treatment as an efficient adsorbent of some important organic dyes. *Green Process. Synth.* **2022**, *11*, 617−630.

(6) Rehman, A. U.; Sharafat, U.; Gul, S.; Khan, M. A.; Khan, S. B.; Ismail, M.; Khan, M. I. Green synthesis of manganese-doped superparamagnetic iron oxide nanoparticles for the effective removal of Pb(ii) from aqueous solutions. *Green Process. Synth.* **2022**, *11*, 287−305.

(7) Kositzi, M.; Antoniadis, A.; Poulios, I.; Kiridis, I.; Malato, S. Solar photocatalytic treatment of simulated dyestuff effluents. *Sol. Energy* **2004**, *77*, 591−600.

(8) (a) Hoffmann, M. R.; Martin, S. T.; Choi, W.; Bahnemann, D. W. Environmental applications of semiconductor photocatalysis. *Chem. Rev.* **1995**, *95*, 69−96. (b) Akhundi, A.; Zaker Moshfegh, A.; Habibi-Yangjeh, A.; Sillanpää, M. Simultaneous dual-functional photocatalysis by g-C3N4-based nanostructures. *ACS ES&T Eng.* **2022**, *2*, 564−585.

(9) (a) Ibhadon, A. O.; Fitzpatrick, P. Heterogeneous photocatalysis: recent advances and applications. *Catalysts* **2013**, *3*, 189−218. (b) El Mously, D. A.; Mahmoud, A. M.; Abdel-Raoof, A. M.; Elgazzar, E. Synthesis of Prussian Blue Analogue and Its Catalytic Activity toward Reduction of Environmentally Toxic Nitroaromatic Pollutants. *ACS Omega* **2022**, *7*, 43139−43146.

(10) (a) Miranda-García, N.; Maldonado, M. I.; Coronado, J.; Malato, S. Degradation study of 15 emerging contaminants at low concentration by immobilized TiO2 in a pilot plant. *Catal. Today* **2010**, *151*, 107−113. (b) Ni, M.; Leung, M. K.; Leung, D. Y.; Sumathy, K. A review and recent developments in photocatalytic water-splitting using TiO2 for hydrogen production. *Renewable Sustainable Energy Rev.* **2007**, *11*, 401−425.

(11) Khan, S. B.; Ismail, M.; Bakhsh, E. M.; Asiri, A. M. Design of simple and efficient metal nanoparticles templated on ZnO-chitosan coated textile cotton towards the catalytic reduction of organic pollutants. *J. Ind. Text.* **2020**, *51*, 1703S−1728S.

(12) (a) Jing, H.-Y.; Wen, T.; Fan, C.-M.; Gao, G.-Q.; Zhong, S.-L.; Xu, A.-W. Efficient adsorption/photodegradation of organic pollutants from aqueous systems using Cu 2 O nanocrystals as a novel integrated photocatalytic adsorbent. *J. Mater. Chem. A* **2014**, *2*, 14563−14570. (b) Akhundi, A.; Badiei, A.; Ziarani, G. M.; Habibi-Yangjeh, A.; Munoz-Batista, M. J.; Luque, R. Graphitic carbon nitride-based photocatalysts: toward efficient organic transformation for value-added chemicals production. *Mol. Catal.* **2020**, *488*, No. 110902.

(13) Peng, K.; Fu, L.; Yang, H.; Ouyang, J. Perovskite LaFeO3/montmorillonite nanocomposites: synthesis, interface characteristics and enhanced photocatalytic activity. *Sci. Rep.* **2016**, *6*, No. 19723.

(14) Keane, D.; Basha, S.; Nolan, K.; Morrissey, A.; Oelgemöller, M.; Tobin, J. M. Photodegradation of famotidine by integrated photocatalytic adsorbent (IPCA) and kinetic study. *Catal. Lett.* **2011**, *141*, 300−308.

(15) Li, L.; Zhao, L.; Ma, J.; Tian, Y. Preparation of graphene oxide/chitosan complex and its adsorption properties for heavy metal ions. *Green Process. Synth.* **2020**, *9*, 294−303.

(16) (a) Habte, A. T.; Ayele, D. W. Synthesis and characterization of reduced graphene oxide (rGO) started from graphene oxide (GO) using the tour method with different parameters. *Adv. Mater. Sci. Eng.* **2019**, *2019*, 1−9. (b) Bai, S.; Shen, X. Graphene−inorganic nanocomposites. *RSC Adv.* **2012**, *2*, 64−98.

(17) Wu, C.-H.; Wang, C.-H.; Lee, M.-T.; Chang, J.-K. Unique Pd/graphene nanocomposites constructed using supercritical fluid for superior electrochemical sensing performance. *J. Mater. Chem.* **2012**, *22*, 21466−21471.

(18) Dong, L.; Gari, R. R. S.; Li, Z.; Craig, M. M.; Hou, S. Graphene-supported platinum and platinum−ruthenium nanoparticles with high electrocatalytic activity for methanol and ethanol oxidation. *Carbon* **2010**, *48*, 781−787.

(19) An, X.; Jimmy, C. Y.; Wang, Y.; Hu, Y.; Yu, X.; Zhang, G. WO 3 nanorods/graphene nanocomposites for high-efficiency visible-light-driven photocatalysis and NO 2 gas sensing. *J. Mater. Chem.* **2012**, *22*, 8525−8531.

(20) Kim, H.; Seo, D.-H.; Kim, S.-W.; Kim, J.; Kang, K. Highly reversible Co3O4/graphene hybrid anode for lithium rechargeable batteries. *Carbon* **2011**, *49*, 326−332.

(21) Low, J.; Yu, J.; Ho, W. Graphene-based photocatalysts for CO2 reduction to solar fuel. *J. Phys. Chem. Lett.* **2015**, *6*, 4244−4251.

(22) Anjum, F.; Asiri, A. M.; Khan, M. A.; Khan, M. I.; Khan, S. B.; Akhtar, K.; Bakhsh, E. M.; Alamry, K. A.; Alfifi, S. Y.; Chakraborty, S. Photo-degradation, thermodynamic and kinetic study of carcinogenic dyes via zinc oxide/graphene oxide nanocomposites. *J. Mater. Res. Technol.* **2021**, *15*, 3171−3191.

(23) Sarkar, C.; Dolui, S. K. Synthesis of copper oxide/reduced graphene oxide nanocomposite and its enhanced catalytic activity towards reduction of 4-nitrophenol. *RSC Adv.* **2015**, *5*, 60763−60769.

(24) Choi, J.; Oh, H.; Han, S.-W.; Ahn, S.; Noh, J.; Park, J. B. Preparation and characterization of graphene oxide supported Cu, Cu2O, and CuO nanocomposites and their high photocatalytic activity for organic dye molecule. *Curr. Appl. Phys.* **2017**, *17*, 137−145.
(25) (a) Xiao, G.; Gao, P.; Wang, L.; Chen, Y.; Wang, Y.; Zhang, G. Ultrasonochemical-assisted synthesis of CuO nanorods with high hydrogen storage ability. *J. Nanomater.* **2011**, *2011*, 1−6. (b) Vila, M.; Diaz-Guerra, C.; Piqueras, J. Optical and magnetic properties of CuO nanowires grown by thermal oxidation. *J. Phys. D: Appl. Phys.* **2010**, *43*, No. 135403.
(26) Sun, H.; Cao, L.; Lu, L. Magnetite/reduced graphene oxide nanocomposites: one step solvothermal synthesis and use as a novel platform for removal of dye pollutants. *Nano Res.* **2011**, *4*, 550−562.
(27) Albukhari, S. M.; Ismail, M.; Akhtar, K.; Danish, E. Y. Catalytic reduction of nitrophenols and dyes using silver nanoparticles @ cellulose polymer paper for the resolution of waste water treatment challenges. *Colloids Surf., A* **2019**, *577*, 548−561.
(28) Kaur, M.; Kaur, H.; Kukkar, D. In *Synthesis and Characterization of Graphene Oxide Using Modified Hummer's Method*, AIP Conference Proceedings, AIP Publishing LLC, 2018; p 030180.
(29) Singh, A.; Singh, N.; Hussain, I.; Singh, H.; Yadav, V. Synthesis and characterization of copper oxide nanoparticles and its impact on germination of Vigna radiata (L.) R. Wilczek. *Tropical Plant Res.* **2017**, *4*, 246−253.
(30) Gayathri, S.; Jayabal, P.; Kottaisamy, M.; Ramakrishnan, V. Synthesis of ZnO decorated graphene nanocomposite for enhanced photocatalytic properties. *J. Appl. Phys.* **2014**, *115*, No. 173504.
(31) Zhang, Y.; Tang, T.-T.; Girit, C.; Hao, Z.; Martin, M. C.; Zettl, A.; Crommie, M. F.; Shen, Y. R.; Wang, F. Direct observation of a widely tunable bandgap in bilayer graphene. *Nature* **2009**, *459*, 820−823.
(32) Sarode, H. A.; Barai, D. P.; Bhanvase, B. A.; Ugwekar, R. P.; Saharan, V. Investigation on preparation of graphene oxide-CuO nanocomposite based nanofluids with the aid of ultrasound assisted method for intensified heat transfer properties. *Mater. Chem. Phys.* **2020**, *251*, No. 123102.
(33) Dhineshbabu, N. R.; Rajendran, V.; Nithyavathy, N.; Vetumperumal, R. Study of structural and optical properties of cupric oxide nanoparticles. *Appl. Nanosci.* **2016**, *6*, 933−939.
(34) (a) Bhaumik, A.; Shearin, A. M.; Patel, R.; Ghosh, K. Significant enhancement of optical absorption through nano-structuring of copper based oxide semiconductors: possible future materials for solar energy applications. *Phys. Chem. Chem. Phys.* **2014**, *16*, 11054−11066. (b) Buazar, F.; Sweidi, S.; Badri, M.; Kroushawi, F. Biofabrication of highly pure copper oxide nanoparticles using wheat seed extract and their catalytic activity: A mechanistic approach. *Green Process. Synth.* **2019**, *8*, 691−702.
(35) Varughese, G.; Rini, V.; Suraj, S.; Usha, K. Characterisation and optical studies of copper oxide nanostructures doped with lanthanum ions. *Adv. Mater. Sci.* **2014**, *14*, 49.
(36) Ismail, M.; Gul, S.; Khan, M.; Khan, M. A.; Asiri, A. M.; Khan, S. B. Medicago polymorpha-mediated antibacterial silver nanoparticles in the reduction of methyl orange. *Green Process. Synth.* **2019**, *8*, 118−127.
(37) Rout, S. Synthesis and Characterization of CuO/Graphene Oxide Composite. Doctoral Dissertation, 2013.
(38) Singh Rathour, R. K.; Bhattacharya, J.; Mukherjee, A. Facile synthesis of graphene oxide for multicycle adsorption of aqueous Pb2+ in the presence of divalent cations and polyatomic anions. *J. Chem. Eng. Data* **2018**, *63*, 3465−3474.
(39) Yao, W.-T.; Yu, S.-H.; Zhou, Y.; Jiang, J.; Wu, Q.-S.; Zhang, L.; Jiang, J. Formation of Uniform CuO Nanorods by Spontaneous Aggregation: Selective Synthesis of CuO, Cu2O, and Cu Nanoparticles by a Solid-Liquid Phase Arc Discharge Process. *J. Phys. Chem. B* **2005**, *109*, 14011−14016.
(40) Messaoudi, O.; Elgharbi, S.; Bougoffa, A.; Mansouri, M.; Bardaoui, A.; Teka, S.; Manai, L.; Azhary, A. Annealing temperature investigation on electrodeposited Cu2O properties. *Phase Transitions* **2020**, *93*, 1089−1099.
(41) Guzman, M.; Arcos, M.; Dille, J.; Rousse, C.; Godet, S.; Malet, L. Effect of the Concentration and the Type of Dispersant on the Synthesis of Copper Oxide Nanoparticles and Their Potential Antimicrobial Applications. *ACS Omega* **2021**, *6*, 18576−18590.
(42) Ganga, B. G.; Santhosh, P. N. Manipulating aggregation of CuO nanoparticles: Correlation between morphology and optical properties. *J. Alloys Compd.* **2014**, *612*, 456−464.
(43) Hamed, M.; Gazwi, H.; Youssif, A. M. Biosynthesis of Copper Oxide Nanoparticles by Marine Streptomyces MHM38 and their Preventive Efficacy Against Paracetamol-Inducing Hepatic Damage of Albino Rats. 2020.
(44) Vasanthi, V.; Logu, T.; Ramakrishnan, V.; Anitha, K.; Sethuraman, K. Study of electrical conductivity and photoelectric response of liquid phase exfoliated graphene thin film prepared via spray pyrolysis route. *Carbon Lett.* **2020**, *30*, 417−423.
(45) Sagadevan, S.; Zaman Chowdhury, Z.; Johan, M. R. B.; Aziz, F. A.; Salleh, E. M.; Hawa, A.; Rafique, R. F. A one-step facile route synthesis of copper oxide/reduced graphene oxide nanocomposite for supercapacitor applications. *J. Exp. Nanosci.* **2018**, *13*, 284−296.
(46) Riaz, M.; Sharafat, U.; Zahid, N.; Ismail, M.; Park, J.; Ahmad, B.; Rashid, N.; Fahim, M.; Imran, M.; Tabassum, A. Synthesis of biogenic silver nanocatalyst and their antibacterial and organic pollutants reduction ability. *ACS Omega* **2022**, *7*, 14723−14734.
(47) Vidhu, V.; Philip, D. Spectroscopic, microscopic and catalytic properties of silver nanoparticles synthesized using Saraca indica flower. *Spectrochim. Acta, Part A* **2014**, *117*, 102−108.
(48) Singh, N. K.; Saha, S.; Pal, A. Methyl red degradation under UV illumination and catalytic action of commercial ZnO: a parametric study. *Desalin. Water Treat.* **2015**, *56*, 1066−1076.
(49) Sahoo, C.; Gupta, A.; Pal, A. Photocatalytic degradation of Methyl Red dye in aqueous solutions under UV irradiation using Ag+ doped TiO2. *Desalination* **2005**, *181*, 91−100.
(50) Mahmoud, M.; Poncheri, A.; Badr, Y.; Abd El Wahed, M. Photocatalytic degradation of methyl red dye. *S. Afr. J. Sci.* **2009**, *105*, 299−303.
(51) Devi, L. G.; Raju, K. A.; Kumar, S. G. Photodegradation of methyl red by advanced and homogeneous photo-Fenton's processes: A comparative study and kinetic approach. *J. Environ. Monit.* **2009**, *11*, 1397−1404.
(52) Nhu, V. T. T.; Hien, N. Q. In *Photodegradation of Methyl Red under Visible Light Using Ag/TiO2 Synthesized by γ-Irradiation Method*, 2016 3rd International Conference on Green Technology and Sustainable Development (GTSD), IEEE: 2016; pp 267−269.
(53) Pouretedal, H.; Sabzevari, S. Photodegradation study of congo red, methyl orange, methyl red and methylene blue under simulated solar irradiation catalyzed by ZnS/CdS nanocomposite. *Desalin. Water Treat.* **2011**, *28*, 247−254.
(54) Jeyabalan, T.; Peter, P. Degradation of dyes (methylene blue and Congo red dye) using phosphomolybdic acid. *Int. J. Sci. Res.* **2014**, *3*, 2312−2315.
(55) Vanaja, M.; Paulkumar, K.; Baburaja, M.; Rajeshkumar, S.; Gnanajobitha, G.; Malarkodi, C.; Sivakavinesan, M.; Annadurai, G. Degradation of methylene blue using biologically synthesized silver nanoparticles. *Bioinorg. Chem. Appl.* **2014**, *2014*, 1−8.
(56) (a) Kiriakidou, F.; Kondarides, D. I.; Verykios, X. E. The effect of operational parameters and TiO2-doping on the photocatalytic degradation of azo-dyes. *Catal. Today* **1999**, *54*, 119−130. (b) Nam, W.; Kim, J.; Han, G. Photocatalytic oxidation of methyl orange in a three-phase fluidized bed reactor. *Chemosphere* **2002**, *47*, 1019−1024.
(57) Fox, M. A.; Dulay, M. T. Heterogeneous photocatalysis. *Chem. Rev.* **1993**, *93*, 341−357.
(58) Reddy, C. B.; Bharti, R.; Kumar, S.; Das, P. Supported palladium nanoparticles-catalyzed decarboxylative coupling approaches to aryl alkynes, indoles and pyrrolines synthesis. *RSC Adv.* **2016**, *6*, 71117−71121.
(59) Anjum, F.; Gul, S.; Khan, M. I.; Khan, M. A. Efficient synthesis of palladium nanoparticles using guar gum as stabilizer and their

https://doi.org/10.1021/acsomega.3c00129
ACS Omega 2023, 8, 17667−17681

applications as catalyst in reduction reactions and degradation of azo dyes. *Green Process. Synth.* **2019**, *9*, 63−76.
(60) Bakhsh, E. M.; Ismail, M.; Sharafat, U.; Akhtar, K.; Fagieh, T. M.; Danish, E. Y.; Khan, S. B.; Khan, M. I.; Khan, M. A.; Asiri, A. M. Highly efficient and recoverable Ag-Cu bimetallic catalyst supported on taro-rhizome powder applied for nitroarenes and dyes reduction. *J. Mater. Res. Technol.* **2022**, *18*, 769−787.
(61) Saien, J.; Soleymani, A. R. Feasibility of using a slurry falling film photo-reactor for individual and hybridized AOPs. *J. Ind. Eng. Chem.* **2012**, *18*, 1683−1688.
(62) Zhao, C.; Pelaez, M.; Dionysiou, D. D.; Pillai, S. C.; Byrne, J. A.; O'Shea, K. E. UV and visible light activated TiO2 photocatalysis of 6-hydroxymethyl uracil, a model compound for the potent cyanotoxin cylindrospermopsin. *Catal. Today* **2014**, *224*, 70−76.
(63) Galindo, C.; Jacques, P.; Kalt, A. Photodegradation of the aminoazobenzene acid orange 52 by three advanced oxidation processes: UV/H2O2, UV/TiO2 and VIS/TiO2: comparative mechanistic and kinetic investigations. *J. Photochem. Photobiol., A* **2000**, *130*, 35−47.
(64) Van Hung, N.; Nguyet, B. T. M.; Nghi, N. H.; Nguyen, V. T.; Binh, T. V.; Tu, N. T. T.; Dung, N. N.; Khieu, D. Q. Visible light photocatalytic degradation of organic dyes using W-modified TiO2/SiO2 catalyst. *Vietnam J. Chem.* **2021**, *59*, 620−638.

NOTE ADDED AFTER ASAP PUBLICATION

This article originally published with two missing reference citations. Reference 22 was added to Section 2.2 and the caption of Figure 4 and the article reposted May 8, 2023.

https://doi.org/10.1021/acsomega.3c00129
ACS Omega 2023, 8, 17667−17681